MIT Open Access Articles

Topological Valley Currents in Gapped Dirac Materials

Massachusetts Institute of Technology

Topological Valley Currents in Gapped Dirac Materials

Yuri D. Lensky,[1] Justin C. W. Song,[2] Polnop Samutpraphoot,[1] and Leonid S. Levitov[1]

[1]*Physics Department, Massachusetts Institute of Technology, Cambridge, Massachusetts 02139, USA*
[2]*Walter Burke Institute for Theoretical Physics and Institute for Quantum Information and Matter,*
California Institute of Technology, Pasadena, California 91125, USA

Gapped 2D Dirac materials, in which inversion symmetry is broken by a gap-opening perturbation, feature a unique valley transport regime. Topological valley currents in such materials are dominated by bulk currents produced by electronic states just beneath the gap rather than by edge modes. The system ground state hosts dissipationless persistent valley currents existing even when topologically protected edge modes are absent. Valley currents induced by an external bias are characterized by a quantized half-integer valley Hall conductivity. The undergap currents dominate magnetization and the charge Hall effect in a light-induced valley-polarized state.

PACS numbers: 72.80.Vp

Bloch bands in materials with broken inversion symmetry can feature Berry curvature, an intrinsic physical field which dramatically impacts carrier transport [1,2]. The key manifestation of Berry curvature is the anomalous Hall effect (AHE), arising in the absence of magnetic field due to topological currents flowing in the system bulk transverse to an applied electric field [3,4]. Of high current interest are Dirac materials with several valleys, such as graphene and transition metal dichalcogenide monolayers [5,6]. Topological currents in these systems have opposite signs in different valleys and, if intervalley scattering is weak, can give rise to long-range charge-neutral valley currents. Such currents have been observed recently in graphene superlattices [7]. Alternatively, if valley polarization is induced by light with nonzero helicity, a charge Hall effect is observed [8].

Topological effects are particularly striking in gapped systems where Chern bands support topologically protected edge modes and quantized transport [9–12]. However, existing valley Hall materials [5–8] lie squarely outside this paradigm. First, gapless edge states in these materials are not enforced by topology or symmetry and may thus be absent. Second, even when present, these states are not protected against backscattering and localization. Naïvely, the lack of edge transport would lead one to conclude that topological currents cease to exist. If true, this would imply that the key manifestations, such as valley Hall conductivity and orbital magnetization, vanish in the gapped state [6].

Here we argue that the opposite is true: the absence of conducting edge modes does not present an obstacle since valley currents can be transmitted by bulk states beneath the gap. As we will see, rather than vanishing, valley currents peak in the gapped state. Further, we will argue that such currents are of a persistent nature, since they represent a ground state property, an integral part of thermodynamic equilibrium. In a valley-polarized state, the undergap currents dominate magnetization and the charge Hall effect.

The effects due to undergap states should be contrasted with those due to deep-lying states which govern field-theoretic anomalies [13,14]. The anomaly-related currents can lead to interesting transport effects such as chiral transport in Weyl semimetals [15,16] and in ^{3}He [17]. Importantly, the deep-lying states in our system obey inversion symmetry and thus do not contribute to valley transport. Indeed, a weak gap-opening perturbation which breaks inversion symmetry at energies near the Dirac point has little impact on deep-lying states. This is quite unlike the anomaly situation where symmetry is broken by regularization at the bandwidth scale but remains intact at lower energies. The regime studied here, where valley currents are dominated by states just beneath the gap, is unique for systems with a weak inversion-breaking perturbation. A similar behavior is expected in systems such as gapped graphene bilayers and twisted double layers.

To gain insight into these delicate issues, we consider a model edge-free gapped system: a *pn* junction in gapped graphene created by a static in-plane electric field; see Fig. 1. This system features an interesting spatial distribution of valley currents which *peak* in the gapped *pn* region $-x_0 < x < x_0$. The origin of such (perhaps counterintuitive) behavior is as follows. Valley currents are due to states just above and just below the gap and, crucially, are of opposite sign for the two groups of states. These states are either both depleted of carriers or both filled away from the gapped region, giving contributions that nearly cancel. This produces a net current decreasing to zero away from the *pn* region; see Eq. (14). In contrast, these contributions are maximally imbalanced in the *pn* region, creating a maximum current which is quantized to a half-integer value per valley $j = (e^2/2h)E$, where E is the in-plane field.

(a)

(b)

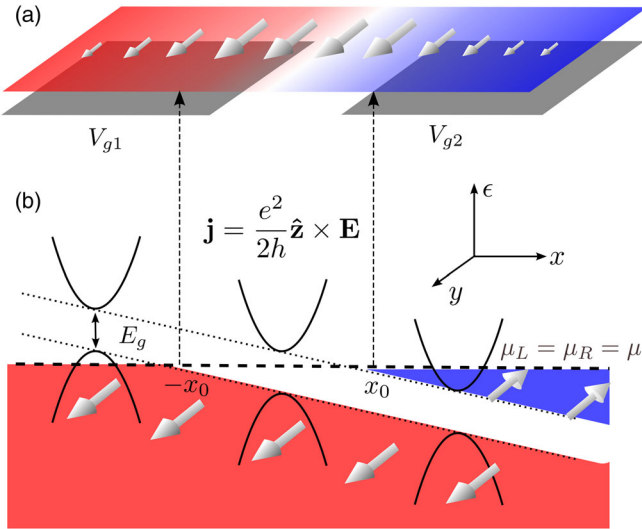$$\mathbf{j} = \frac{e^2}{2h}\hat{\mathbf{z}} \times \mathbf{E}$$

FIG. 1 (color online). Persistent valley currents inside and outside the *pn* junction. The currents arise from side jumps of band carriers just beneath and just above the gap upon reflection from the gapped region, as illustrated by trajectories in Fig. 2. The undergap and overgap currents (red and blue regions) flow in opposite directions and fully cancel deep in the Fermi sea. The two contributions are maximally uncompensated inside the region $-x_0 < x < x_0$, giving a maximum current value of $j = (e^2/2h)E$ per valley, where E is the in-plane electric field.

Our analysis, which is microscopic and explicit, applies equally well to a spatially uniform gapped system under bias (and with no gate-induced built-in fields), predicting a quantized valley Hall effect with $\sigma_{xy} = (e^2/2h)$ per valley. In terms of the arrangement shown in Fig. 1 this corresponds to system sizes L smaller than the gapped region width $2x_0 = E_g/eE$, i.e., weak bias voltage $V = EL \ll E_g/e$. Since valley currents are transmitted by undergap states in the system bulk, they are nondissipative. Below we also discuss valley edge currents resulting from the side jumps of the undergap states upon reflection from system boundary; see Fig. 3. Together with bulk currents, such edge currents ensure the valley flow continuity. These currents circulate along the edge, producing orbital magnetization in the system ground state; see Eq. (15). We note parenthetically that σ_{xy} values become unquantized by intervalley scattering by disorder. However, given the exceptionally long mean free paths in currently studied graphene systems, we expect our ballistic model to be adequate.

We model carriers in each valley as a $2 + 1$ massive Dirac particle in the presence of a static uniform electric field which defines a *pn* junction:

$$H = \begin{pmatrix} \Delta & vp_- \\ vp_+ & -\Delta \end{pmatrix} - eEx, \qquad p_\pm = p_1 \pm ip_2, \quad (1)$$

where $\Delta = E_g/2$ and $p_{1,2}$ denote momentum components $p_{x,y}$. The system ground state is a Fermi sea with a density

gradient imposed by the E field, n doped on one side and p doped on the other side of a gapped region; see Fig. 1. Simple as it is, the above Hamiltonian captures all essential elements of interest: tunneling through the gapped region, AHE in surrounding regions, and their interplay.

We tackle Eq. (1) by mapping it onto a fundamental problem in quantum dynamics: a pair of quantum levels driven through an avoided level crossing. The Landau-Zener (LZ) problem describing these transitions admits an exact solution [18,19]. As we will see, the LZ framework fully accounts for the AHE transport. Below we discuss the relation between our LZ approach and the conventional quasiclassical approach based on the adiabatic theorem and Berry phase [1,2]. Since the LZ approach is not restricted to the adiabatic limit, it gives a full account of nonadiabatic effects associated with tunneling through the gapped region in our transport problem. Such effects, which are naturally described in the LZ framework, are not accounted for by the quasiclassical approach.

Mapping of Eq. (1) onto the LZ problem proceeds in two steps. We first note that in the momentum representation $\varepsilon\psi = H\psi$ is a first-order differential equation, since the only term containing a derivative is $-eEx = eEi\hbar\partial_{p_1}$. We can thus rewrite our equation as a time-dependent Schrödinger equation for a 2×2 Hamiltonian, with $t = p_1/eE$ playing the role of time:

$$i\hbar\partial_t\psi(t) = \tilde{H}(t)\psi(t), \quad \tilde{H}(t) = \beta t\sigma_1 + vp_2\sigma_2 + \Delta\sigma_3. \quad (2)$$

Here we set $\varepsilon = 0$ without loss of generality and defined $\beta = veE$. Next, by interchanging spin components via $\sigma_1 \leftrightarrow \sigma_3$, $\sigma_2 \rightarrow -\sigma_2$ we bring $\tilde{H}$ to the canonical LZ form

$$\tilde{H}(t) = \begin{pmatrix} \beta t & \Delta_p \\ \Delta_p^* & -\beta t \end{pmatrix}, \qquad \Delta_p = \Delta + ivp, \quad (3)$$

where from now on we use p instead of p_2 for brevity.

Time evolution in Eq. (2) defines a unitary S matrix which takes its simplest form in the adiabatic basis of instantaneous eigenstates of $\tilde{H}(t)$. These states correspond to a particle moving in a classically allowed region, p or n, without tunneling through the gapped region. Tunneling is thus described by the LZ transitions between different adiabatic states. Written in the adiabatic basis, the S matrix is of the form

$$S = \begin{pmatrix} \sqrt{q} & -\sqrt{1-q}e^{i\varphi} \\ \sqrt{1-q}e^{-i\varphi} & \sqrt{q} \end{pmatrix}, \qquad q = e^{-2\pi\delta}, \quad (4)$$

where $\delta = |\Delta_p|^2/2\beta\hbar$. Here the phase φ is given by [20]

$$\varphi = \pi/4 + \arg\Gamma(1 - i\delta) + \delta(\ln\delta - 1) + \arg\Delta_p \quad (5)$$

with $\Gamma(z)$ the Gamma function. The nonadiabatic and adiabatic LZ transitions, taking place with the probabilities

q and $1 - q$, correspond to particle transmission through the gapped region and reflection from it. The evolution is adiabatic at small β, i.e., at a weak E field. In this case, the system tracks one of the instantaneous eigenstates of $\tilde{H}(t)$ whereas nonadiabatic transitions describe tunneling. Such transitions are exponentially suppressed at small β.

Importantly, the S matrix exhibits features expected for the AHE transport. In particular, it predicts side jumps— transverse particle displacement induced by its proximity to the pn region. We evaluate the y displacement as $\langle \delta y \rangle = \langle \psi | i\hbar \partial_p | \psi \rangle$, with the expectation value taken over the left- and right-incident states $|L\rangle = S \begin{pmatrix} 1 \\ 0 \end{pmatrix}$, $|R\rangle = S \begin{pmatrix} 0 \\ 1 \end{pmatrix}$. We find

$$\langle \delta y \rangle_{L,R} = \pm \frac{\partial \varphi}{\partial p} = \pm \ell (1 - q), \quad \ell = \frac{\hbar v \Delta}{|\Delta_p|^2}, \quad (6)$$

where only the last term of the phase in Eq. (5), which is even in p, gives a contribution to the net valley current. Interestingly, the result in Eq. (6) only depends on $1 - q$ that corresponds to reflection, indicating that side jumps occur only at reflection from the gapped region but not in transmission through it. The side-jump direction reverses upon Δ sign reversal. Valley K and K' contributions are of opposite sign as expected for valley Hall transport.

Encouraged by these observations, we proceed to construct individual one-particle quantum states exhibiting side jumps. Since Dirac particle velocity is expressed through its spin $\mathbf{v} = (1/i\hbar)[\mathbf{x}, H] = v(\sigma_1, \sigma_2)$, it will be convenient to represent LZ dynamics as spin-1/2 evolution. The latter is described by the Bloch equation for magnetization vector $\mathbf{m}(t) = \langle \psi(t) | \mathbf{s} | \psi(t) \rangle$, $s_i = (\hbar/2)\sigma_i$,

$$\partial_t \mathbf{m} = \mathbf{b}(t) \times \mathbf{m}, \quad \mathbf{b}(t) = \frac{2}{\hbar}(\Delta, -vp, \beta t) \quad (7)$$

where the magnetic field $\mathbf{b}(t)$ orientation changes gradually from $-z$ to $+z$ over $-\infty < t < \infty$.

We focus on the weak field regime $eE \ll \Delta/\ell = \Delta^2/\hbar v$. In the LZ formulation (3) this corresponds to spin $1/2$ evolving in a slowly changing magnetic field $\mathbf{b}(t)$ which rotates in the plane perpendicular to the vector

$$\mathbf{n} = (\sin \alpha, \cos \alpha, 0), \quad \tan \alpha = vp/\Delta. \quad (8)$$

Crucially, the adiabatic spin evolution in a rotating field $\mathbf{b}(t)$ can generate a component of $\mathbf{m}$ (and thus of the velocity) transverse to the rotation plane and thus *pointing along* $\mathbf{n}$. This happens because when the field rotates in the plane perpendicular to $\mathbf{n}$ the spin tries to follow it but is left slightly behind. Then, as a result of Bloch precession, the spin rotates out of the plane swept by $\mathbf{b}(t)$;
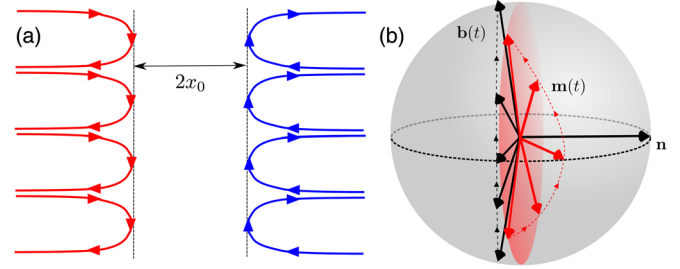

FIG. 2 (color online). (a) The undergap and overgap trajectories near the gapped region, Eq. (13). Skewed Hall-like motion gives rise to side jumps. Shown are normally incident trajectories for electrons and holes. The opposite-flowing undergap and overgap currents partially cancel when summed over all filled states, producing net currents flowing in the same direction in the p and n regions, with the maximum current attained in the middle region $-x_0 < x < x_0$; see Eq. (14) and Fig. 1. (b) Spin-1/2 interpretation of side jumps. Magnetization $\mathbf{m}(t)$ evolves adiabatically in a slowly varying field $\mathbf{b}(t)$ that sweeps a plane perpendicular to $\mathbf{n}$; see Eq. (7). Magnetization tracks the field but lags slightly behind, rotating out of the plane and acquiring a component parallel to $\mathbf{n}$; see Eq. (11). So does the velocity vector which is aligned with $\mathbf{m}(t)$.

see Fig. 2. The transverse component is proportional to rotation speed, i.e., is not exponentially small in the adiabatic limit.

Such a behavior, while somewhat counterintuitive, can be understood as follows. We usually think of a spin precessing in a strong but slowly changing magnetic field as being "slaved to the field." This is basically correct; however, the spin excursions away from the field direction can be nonexponential due to Berry curvature effects. This is precisely the case in our problem.

It is convenient to use a (nonuniformly) rotating frame in which the field $\mathbf{b}(t)$ has a frozen orientation. We write $|\psi(t)\rangle = U(t)|\psi'(t)\rangle$ with the unitary transformation $U(t)$ chosen so that the field $\mathbf{b}'(t)$ defined by $U^{-1}(t)(\mathbf{b}(t) \cdot \mathbf{s})U(t) = \mathbf{b}'(t) \cdot \mathbf{s}$ is directed along a fixed axis. For the Hamiltonian in Eq. (3) the operator $U(t)$ with this property can be defined as a spin rotation

$$U(t) = e^{(i/\hbar)\theta(t)\mathbf{n} \cdot \mathbf{s}}, \quad \tan \theta(t) = \beta t/|\Delta_p|, \quad (9)$$

where $\theta(t)$ is the angle between vectors $\mathbf{b}(t)$ and $\mathbf{b}(0)$. In the rotated frame our equations read

$$i\hbar \partial_t |\psi'(t)\rangle = (\mathbf{b}'(t) \cdot \mathbf{s} - i\hbar U^{-1}(t)\dot{U}(t))|\psi'(t)\rangle. \quad (10)$$

The last term equals $-i\hbar U^{-1}(t)\dot{U}(t) = (\partial \theta(t)/\partial t)\mathbf{n} \cdot \mathbf{s}$ giving a spin Hamiltonian with an effective field $\mathbf{b}'(t) + (\partial \theta(t)/\partial t)\mathbf{n}$.

So far our analysis has been completely general; now, we specialize to an adiabatic evolution in which the spin orientation tracks the field. In this case, when viewed in our rotated frame, $\mathbf{m}(t)$ remains aligned with the vector

$\mathbf{b}'(t) + (\partial\theta(t)/\partial t)\mathbf{n}$ at all times. Transforming back to the lab frame, we conclude that $\mathbf{m}(t)$ tracks the field

$$\tilde{\mathbf{b}}(t) = \mathbf{b}(t) + \frac{\partial\theta(t)}{\partial t}\mathbf{n} \qquad (11)$$

which, because of the last term, has an additional y component. Finally, since the velocity operator $\mathbf{v} = v(\sigma_1, \sigma_2)$ expectation value is aligned with $\mathbf{m}$, the velocity components are easily evaluated as $\mathbf{v}_{x,y} = v\tilde{\mathbf{b}}_{x,y}/|\tilde{\mathbf{b}}|$ giving

$$v_x(t) = \frac{v\beta t}{\varepsilon(t)}, \qquad v_y(t) = \frac{v^2 p}{\varepsilon(t)} + \frac{v\Delta\beta}{2\varepsilon^3(t)}, \qquad (12)$$

where $\varepsilon(t) = \pm\sqrt{\beta^2 t^2 + |\Delta_p|^2}$ with the plus (minus) sign describing the p (n) state. Here we normalized $\tilde{\mathbf{b}}(t)$ approximating $|\tilde{\mathbf{b}}(t)| \approx |\mathbf{b}(t)|$. Trajectories are readily obtained by integrating velocity, giving

$$x(t) = \frac{v\varepsilon(t)}{\beta}, \qquad y(t) = \frac{v^2 p}{|\Delta_p|}\ln\frac{\varepsilon(t) + \beta t}{|\Delta_p|} + \frac{v\Delta\beta t}{2|\Delta_p|^2\varepsilon(t)} \qquad (13)$$

(here we suppressed integration constants). The last term in Eqs. (12) and (13) originates from Berry curvature, giving rise to side jumps; see Fig. 2. The net side-jump value is $\delta y = \int_{-\infty}^{\infty} v_y(t)dt = v\Delta/|\Delta_p|^2$, which matches the result found above.

These results are in accord with the classical equations of motion augmented with the anomalous velocity term describing the nonclassical Berry's "Lorentz force" [1,2]:

$$\dot{\mathbf{p}} = e\mathbf{E}, \qquad \dot{\mathbf{x}} = \nabla_{\mathbf{p}}\varepsilon_{p,\pm} + \Omega_p \times \dot{\mathbf{p}}, \qquad \Omega_p = \frac{v^2\Delta}{2\varepsilon^3_{p,\pm}},$$

where $\varepsilon_{p,\pm} = \pm(v^2\mathbf{p}^2 + \Delta^2)^{1/2}$ is particle dispersion. Current density, found by summing the velocity contributions of all states in the Fermi sea, is

$$j(x) = \begin{cases} j_0 & |x| < x_0 \\ j_0 x_0/|x| & |x| > x_0, \end{cases} \qquad j_0 = \frac{e^2}{2h}E \quad (14)$$

per valley. The current peaks in the gapped region, falling off inversely with distance outside this region, as shown in Fig. 1(a). An identical result is obtained by integrating the velocity in Eq. (12) over allowed values of p. As discussed above, this current $j(x)$ originates from side jumps of undergap trajectories, whereas the decrease of $j(x)$ at $|x| > x_0$ accounts for partial cancellation between the overgap and undergap side jumps. Equation (14) predicts a universal, E-independent net current flowing through the gapped region $I_{|x|<x_0} = e\Delta/\hbar$.

Dissipationless currents in a spatially uniform gapped system can also be created by a voltage bias. Indeed, the microscopic transport picture under a weak bias (and no gate-induced built-in fields) is well described by the above model, so long as $eE_{\text{bias}} \ll \Delta/L$ where L is the system size. Our analysis then predicts a universal valley Hall conductivity $\sigma_{xy} = (e^2/2h)$ per valley. Since valley currents in this case are transmitted solely by undergap states in the system bulk, they are nondissipative.

Another interesting phenomenon is *persistent edge currents* in a spatially uniform unbiased gapped system. These currents arise due to side jumps of the undergap states scattered off system edges; see Fig. 3. Circulating along the edge, the currents produce orbital magnetization in the system ground state. Valley K and K' contributions are of opposite sign, giving zero net magnetization in thermodynamic equilibrium. Finite magnetization can be created by using light of a particular helicity to polarize valleys (as in the valley Hall effect measurements [6,8]). We analyze the total magnetic moment

$$M = \int \frac{d^2 r}{2c}\mathbf{r} \times \mathbf{j}(\mathbf{r}) \approx A\frac{\gamma e\Delta}{\hbar c}\sum_{p,i,\pm}\Omega_p n_{i,F}[\varepsilon_{p,\pm}], \quad (15)$$

where A is the system area, $n_{i,F}$ are the Fermi functions with i labeling valleys, and $\gamma \sim 1$ is a numerical constant accounting for edge current suppression due to intervalley scattering induced by edge roughness. This estimate was obtained from considering current I circulating around the sample with the typical side-jump value $\hbar v/\Delta$ found above (in the narrow p-n junction limit). The dependence on the Fermi level arises from summing the contributions of all filled states. Magnetization (magnetic moment per area) attains maximum value when the Fermi level lies inside the gap; see Fig. 3. We estimate the maximum value for each valley and spin projection to be

$$m = M/A \approx e\Delta/2\hbar c = 12.8 \times (\Delta[\text{eV}])\mu_B/(\text{nm})^2, \quad (16)$$
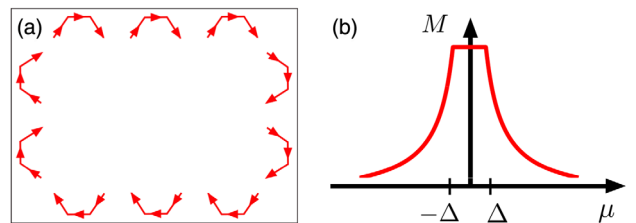

FIG. 3 (color online). (a) Persistent valley currents in a spatially uniform gapped system with the Fermi level inside the gap. Currents arise due to side jumps of the undergap trajectories bouncing off the system boundary. Persistent currents circulate along the edge, giving rise to a constant magnetization per valley, Eq. (15). (b) Orbital magnetization—Eq. (15)—as a function of chemical potential. Magnetization peaks for the Fermi level inside the gap and decreases at large detuning as a result of compensation from overgap and undergap contributions.

where we have taken the maximum value of Berry flux $=$ $1/2$ that occurs in the gap (for a single valley), and used $\gamma = 1$. Here μ_B is the Bohr magneton. For graphene stacked on hexagonal boron nitride, gap sizes can be as large as several tens of meV [7], yielding values of m of $\gtrsim 0.13\,\mu_B/(\text{nm})^2$; larger gap sizes $\Delta \gtrsim 1$ eV in transition metal dichalcogenides will yield correspondingly larger values of magnetization. In 2D systems, magnetization can be measured with torque magnetometry techniques, allowing access to values as low as $0.1\,\mu_B$ per two-dimensional unit cell [21].

Summing up, topological valley currents in gapped materials are transmitted by undergap bulk states rather than by edge modes. The lack of an edge contribution, which is not protected by topology or symmetry, does not present an obstacle since the undergap currents can give rise to dissipationless transport in the gapped state. The undergap currents generate persistent (magnetization) currents in the thermodynamic ground state, flowing in the system bulk and along boundaries. We predict that the key manifestations and observables, such as the valley Hall conductivity and orbital magnetization in valley-polarized systems, reach maximum value in the gapped state. The requirements for observing dissipationless valley transport can be met under realistic conditions.

[1] N. Nagaosa, J. Sinova, S. Onoda, A. H. MacDonald, and N. P. Ong, Rev. Mod. Phys. **82**, 1539 (2010).
[2] 5. D. Xiao, M.-C. Meng, and Q. Niu, Rev. Mod. Phys. **82**, 1959 (2010).
[3] G. Sundaram and Q. Niu, Phys. Rev. B **59**, 14915 (1999).
[4] F. D. M. Haldane, Phys. Rev. Lett. **93**, 206602 (2004).
[5] D. Xiao, G.-B. Liu, W. Feng, X. Xu, and W. Yao, Phys. Rev. Lett. **108**, 196802 (2012).
[6] D. Xiao, W. Yao, and Q. Niu, Phys. Rev. Lett. **99**, 236809 (2007).
[7] R. V. Gorbachev *et al.*, Science **346**, 448 (2014).
[8] K. F. Mak, K. L. McGill, J. Park, and P. L. McEuen, Science **344**, 1489 (2014).
[9] C. L. Kane and E. J. Mele, Phys. Rev. Lett. **95**, 226801 (2005).
[10] B. A. Bernevig, T. L. Hughes, and S. C. Zhang, Science **314**, 1757 (2006).
[11] L. Fu, C. L. Kane, and E. J. Mele, Phys. Rev. Lett. **98**, 106803 (2007).
[12] R. Roy, Phys. Rev. B **79**, 195322 (2009).
[13] S. L. Adler, Phys. Rev. **177**, 2426 (1969).
[14] J. S. Bell and R. Jackiw, Nuovo Cimento A **60**, 47 (1969).
[15] K. Fukushima, D. E. Kharzeev, and H. J. Warringa, Phys. Rev. D **78**, 074033 (2008).
[16] S. A. Parameswaran, T. Grover, D. A. Abanin, D. A. Pesin, and A. Vishwanath, Phys. Rev. X **4**, 031035 (2014).
[17] T. D. C. Bevan, A. J. Manninen, J. B. Cook, J. R. Hook, H. E. Hall, T. Vachaspati, and G. E. Volovik, Nature (London) **386**, 689 (1997).
[18] L. D. Landau, Phys. Z. Sowjetunion **2**, 46 (1932).
[19] C. Zener, Proc. R. Soc. A **137**, 696 (1932).
[20] Y. Kayanuma, Phys. Rev. A **50**, 843 (1994).
[21] L. Li, C. Richter, J. Mannhart, and R. C. Ashoori, Nat. Phys. **7**, 762 (2011).